International Journal of Engineering Research and Modern Education (IJERME)
Impact Factor: 6.525, ISSN (Online): 2455 - 4200
(www.rdmodernresearch.com) Volume 2, Issue 1, 2017

SYNTHESIS OF PURE AND (Mn, Co) CO-DOPED ZnO NANOPARTICLES BY DC THERMAL PLASMA METHOD FOR ETHANOL SENSOR FABRICATION

Dr. M. Nirmala* & Dr. A. Anukaliani**

* Assistant Professor, Department of Physics, Sri GVG Visalakshi College for Women, S.V Mills post, Udumalpet, Tamilnadu

** Associate Professor, PG and Research Department of Physics, Kongunadu Arts and Science College, Coimbatore, Tamilnadu

Cite This Article: Dr. M. Nirmala & Dr. A. Anukaliani, "Synthesis of Pure and (Mn, Co) Co-Doped ZnO Nanoparticles by DC Thermal Plasma Method for Ethanol Sensor Fabrication", International Journal of Engineering Research and Modern Education, Volume 2, Issue 1, Page Number 132-138, 2017.

Abstract:

Ethanol gas sensing characteristics of semiconductor type gas sensors with channels composed of pure and (Mn, Co) co-doped ZnO nanoparticles were investigated in this study. The morphology and structure of ZnO nanostructures were characterized by X-ray diffraction (XRD), scanning electron microscopy (SEM). Compared with high temperature sintered ZnO nanoparticles, low temperature sintered ZnO nanoparticles have better sensibility. The main advantages of these sensors are featured in the excellent selectivity, fast and high response (sensitivity) to ethanol.

Key Words: ZnO, Annealing, Ethanol, Sensors, Doping & Thermal plasma

1. Introduction:

In the field of gas sensors, it is well known that ethanol vapor is one of the most exhaustively studied gases. Metal oxide semiconductor, usually representing a property that the electrical conductivity varies with the composition of the gas atmosphere surrounding it is a popular and useful sensing material for ethanol vapor sensing. Many researchers have developed ethanol vapor sensors based on semiconductor metal oxide. Several oxide materials commonly used as ethanol gas sensors including pure and metal-doped e.g. SnO2 [1], In2O3 [2], TiO2 , ZrO2 [3], WO3 [4], MoO3 [5], Cu2O [6], and ZnO [7], especially ZnO is known to be one of the earliest discovered and the most widely applied oxide gas sensing material.

Zinc oxide (ZnO) is an *n*-type semiconductor of wurtzite structure, with a direct large-band gap of about 3.37 eV at low temperature and 3.30 eV at room temperature. It is sensitive to many sorts of gases at moderate temperature, especially for ethanol vapor [8]. ZnO is one of the most widely applied oxide-gas sensor. ZnO gas sensing materials owe to their high chemical stability, low cost, and good flexibility in fabrication. ZnO sensor elements have been fabricated in various forms including single crystal [7], sinter pellet [9], thin film [10], and thick film [11]. The gas sensing mechanism involves chemisorptions of oxygen on the oxide surface followed by charge transfer during the reaction between chemisorbed oxygen reducing and target gas molecules. However, the physical and sensing properties of semiconductor gas sensors are directly related to their preparation e.g. particle size, sensing film morphology, and film thickness [12-15] as well as sensing film characteristics. In the present study we have used thin pellet of pure and (Mn,Co) co-doped zinc oxide nanopowder synthesized dc thermal plasma method and the sensing response of nanoparticles when subjected to different ethanol concentrations and sintered temperatures are also investigated.

2. Experimental:

Pure and co-doped ZnO (Mn, Co) nanoparticles were synthesized using DC thermal plasma method. The apparatus consist of a DC generator, a plasma torch, a reaction tube, a chamber, a powder feeder and an injection block. Atmospheric air was employed as the plasma gas. Atmospheric air was introduced into the reaction tube with a flow rate of 3 l/min. An oxidation reaction took place in the flame of the plasma. Commercially available Zn metal powder with average particle size of 10-15µm was injected into the plasma region through the powder feeder. The powder was readily evaporated and oxidized by the high temperature of the plasma flame followed by the rapid condensation in the reaction tube wall. The prepared powder was collected from hood and chamber part [16].

Experimental Conditions for the Preparation of ZnO Nanopowders:

Plasma Power	:	7 KW
Open Circuit Voltage (OCV)	:	369V
Type of gas	:	Atmospheric air
Flow rate of the gas	:	3 l/min
Feeding rate of the material	:	Zn metal powder, 20gram
Reaction time	:	4 min

The morphology and crystalline nature of pure and co-doped ZnO are investigated with scanning electron microscope (HITACHI S-3400) and X-ray diffraction (Schimadzer XRD-6000) respectively. Keithley 236 source measure unit attached with an indigenously designed and four probe sample holder was used to study the DC characteristics of the undoped and (Mn, Co) co-doped ZnO nanoparticles in the range of 25-100°C with steps of 25°C. Samples prepared in the form of circular pellets of diameter 0.8cm and 0.4cm thickness for the DC characteristics and annealing effects on ZnO nano materials at different temperatures have also been studied.

3. Results and Discussion:

X-ray diffraction studies confirmed that the synthesized materials are wurtzite phase of ZnO and all the crystal structures agreed with the reported JCPDS data (card No.5-664)[17]. Figure 1 shows the XRD pattern of undoped and (Mn, Co)co-doped ZnO nanopowder.

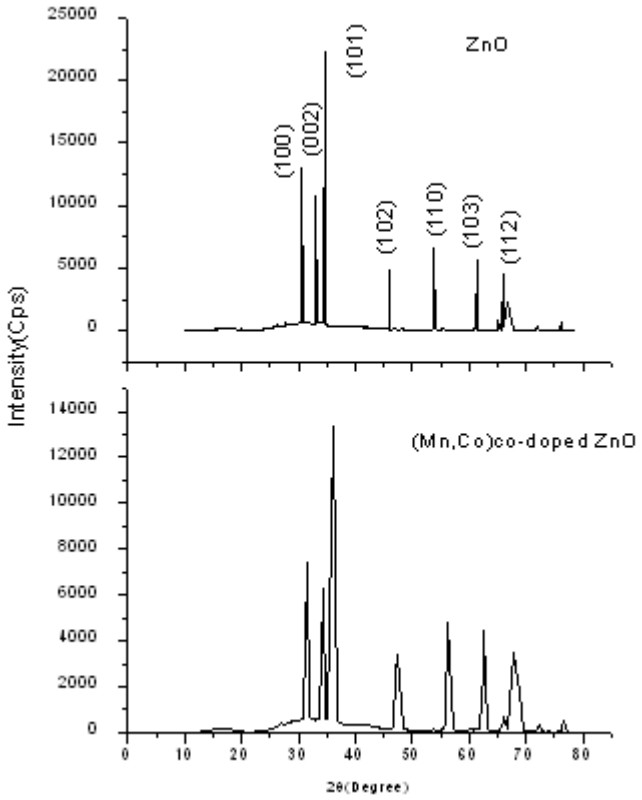

Figure 1: XRD pattern of pure and (Mn, Co)co-doped ZnO Nano powder

A definite line broadening of the diffraction peaks is an indication that the synthesized materials are in nanometer range. The crystallite size was calculated from Scherrer formula applied to the major peaks and was found to be around 25nm and 18nm for undoped ZnO powder and (Mn, Co) co-doped ZnO nanopowders respectively. The lattice parameters calculated are also in accordance with the reported value [17].

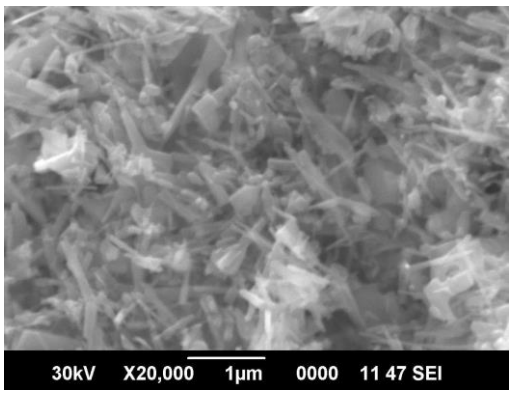

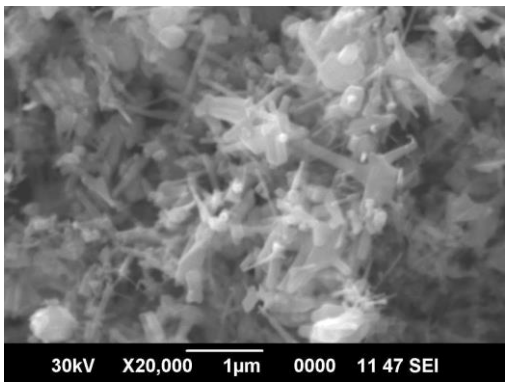

Figure 2a Figure 2b

SEM Image of pure and (Mn,Co) co-doped ZnO Nano powder

Figures 2a and 2b shows the SEM images of undoped and (Mn, Co) co-doped ZnO nanopowders. SEM studies show that the materials are networks of rod-like crystals. The structures obtained are similar to the structure reported by So-Jung Kim et.al [16] for undoped ZnO prepared by thermal plasma method. The morphology of ZnO material in the form of pellet was also investigated. Heat treatment of the ZnO element at different temperatures gave different morphology of the material.

Fig.2c & 2d shows the morphology of undoped and (Mn, Co) co- doped ZnO in the form of pellet annealed at 450°C. It is found that with increase in temperature, material has become more porous. SEM studies show that the material has networks of nanosheet [18].

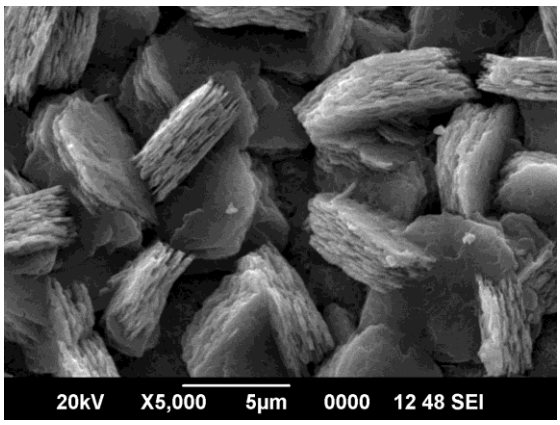

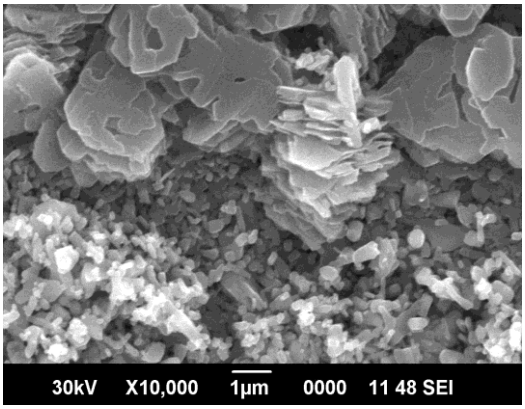

Figure 2c Figure 2d

SEM Image of pure and (Mn,Co) co-doped ZnO pellet

Temperature dependence of conductivity for n-type semiconductor material can be expressed as,

$$\sigma = \sigma_0 e^{-Ea/KT} \quad (1)$$

Where $\sigma_0 = 2\ e\mu_e(2\Pi m_e^*(KT/h^2))^{3/2}$ and $E_a = E_c - E_i$. Here m_e^* is the effective mass and μ_e is the mobility of electron. E_a, E_c and E_i are the energy value corresponding to activation of electronic transport, bottom edge of the conduction band and level of the donor state. T is the absolute temperature of material, e is the electronic charge, h is Planck's constant and k is the Boltzmann constant. In terms of resistance Eq. (1) is given by

$$R = R_0 e^{Ea/KT} \quad (2)$$

From the resistance temperature plot (fig3) in the form of ln(R) versus 1/T the slope gives the value of (E_a/k) of Eq. (2) and from it the activation energy of electronic transport for semi conducting material can be calculated [19-21].

One of the important variables resulting from the electric properties of semiconductors is the activation energy. This is the initial energy that the electric charges need to move inside the material. Activation energy increases with temperature in insulators and semiconductors and decreases in metals. It is well known that electrical conduction can take place by means of two parallel processes namely band conduction and hoping conduction. The band conduction occurs when the carriers are excited beyond the mobility edges into non-localized states at high temperatures. The excitations of carriers into localized states at band edges cause the hoping conduction [22].

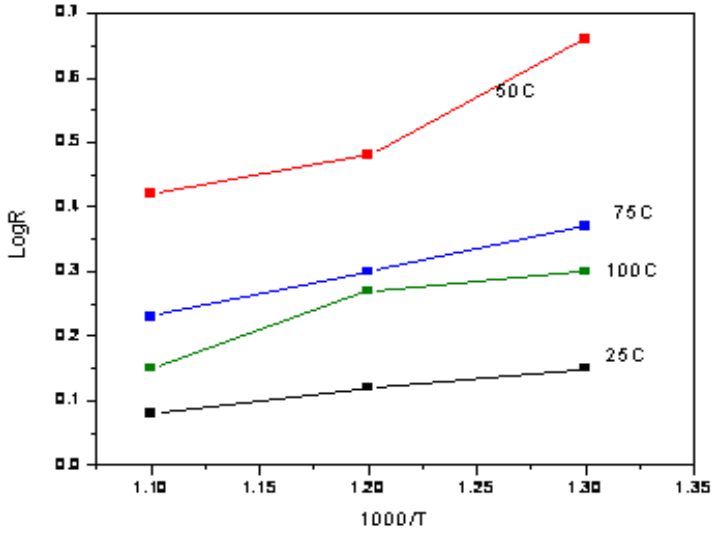

Figure 3: Activation energy plot for ZnO pellet annealed at 450°C

The activation energy for electronic conduction of the ZnO nano-material increases with an increase in temperatures given to the sample. This is possible due to change in surface chemical structure of oxide. The removal of defects in crystallites due to the increase in activation energy with the rise in annealing temperatures. It is also observed that as the annealing temperature increases the resistance of the material decreases. This is probably due to growth crystallites. At any temperature the Gibb's free energy of a crystal is minimum when a certain fraction of ions leaves the normal lattice. Yadav et al [23, 18] has reported that the sample annealed at higher temperature follow conduction of proton by hopping mechanism due to inadequate number of free hydroxyl groups on the surface having higher value of activation energy.

The increase in activation energy gives clue regarding the diffusion of impurities to the regular position or to the interstice [24]. High value of the activation energy may be associated with ionization of deep donor or acceptor levels which become more important at higher temperature. With increasing temperature the concentration of conducting electrons increased and therefore the role of mutual interaction between electrons and donor or acceptor centers become more important [25].

Doping on semiconductor can modify resistance. The electrical conductivity increases with the increase in impurity concentration and temperature. The defect concentration will increase exponentially with temperature and consequently the electrical conduction also increases. The addition of impurity further increases the electrical conduction in the temperature region considered.

Device Fabrication:

The schematic diagram for measuring sensitivity of the sensor is shown in fig.4. The sensing material is placed inside an airtight chamber of known volume 25.000cm^3. The pellet is kept at a room temperature and two Al electrodes are placed on the surface of the pellet, which makes ohmic contact with the pellet. Gas injection is carried out using a hypodermic syringe. Initially the chamber is evacuated to a base pressure of 10^{-2} Torr using a rotary pump and electrical measurements are performed at a room temperature. The response is considered as a reference response for calculation of sensitivity. The test gas is injected inside the bell jar through a needle valve. After injecting the test gas, all the valves are closed to avoid the leakage of test gas.

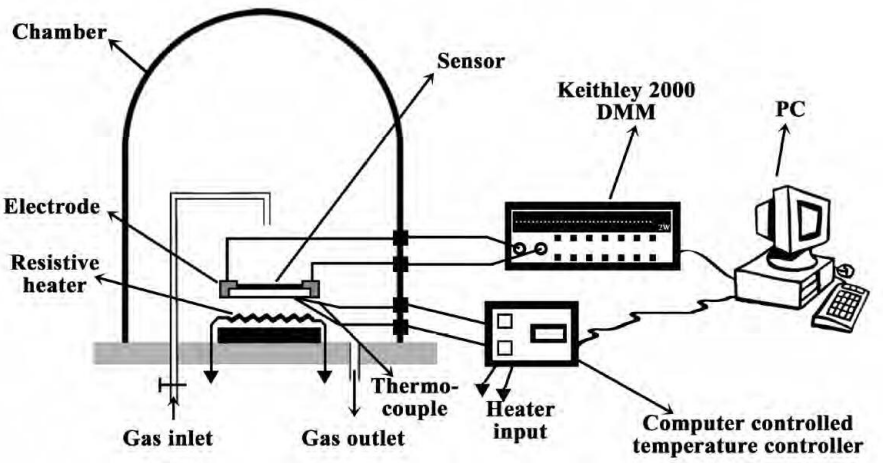

Figure 4: Schematic diagram of ethanol sensor

The resistance of the sensor is once again measured at the same temperature in ethanol vapor ambient. After completing measurements, the gas is wiped off to carryout next cycle by injecting fresh air into the chamber.

Sensor measurement has been performed to monitor the response to ethanol from 100-400ppm which is shown Fig. 5(a), (b) &(c). Fig. 6 shows the sensitivity versus response time and ethanol concentrations plots of undoped and (Mn, Co) co-doped ZnO annealed at 450°C and 550°C respectively. The sensitivities of all sensors were found to increase rather linearly with increasing ethanol concentrations. Nanoparticles have the largest specific surface area, which can maximize the response, subjecting them to heat treatment at high temperatures are unfavorable for fabricating gas sensors. The reason for this is that the infiltration of the target gas molecules into the sample agglomerates and their adsorption and desorption on the surface of the inner particles are inhibited in the case of the agglomerated structures resulting from the high temperature heat treatment. However, in the case of the gas sensors fabricated herein, these problems were overcome by using a relatively low temperature heat treatment process, which makes it possible to fabricate gas sensors with a sparse distribution of the nanoparticles without any agglomeration, in which 1-D structures are formed that enable the target gas molecules to maintain their degree of diffusion into the gaps between the nanoparticles and be easily

adsorbed on their surface. Use of low temperature heat treatment process is the reason why our gas sensors have high detectability [26].

Ethanol sensing mechanism of the ZnO sensors has also been reported in our previous studies [27]. However, only few studies indicate that ZnO has higher gas response to ethanol than other commonly used gases [28]. Most metal oxide semiconductor gas sensors are based on the conductance change arising from the reactions between the oxygen ions and the detecting gas molecules adsorbed on the active surface [29, 30]. It is seen that the electron donating effect of the testing gas molecule is an important factor in the explanation of this phenomenon (In the several forms of oxygen adsorbates, the O^- is more active form of adsorbed oxygen.). For example, the typical testing gas sensing reactions are expressed as follows:

$$CO+O^- \rightarrow CO_2+e^- \quad (1)$$

$$H_2+O^- \rightarrow H_2O+e^- \quad (2)$$

$$HCHO+2O^- \rightarrow H_2O+CO_2+2e^- \quad (3)$$

Catalytic oxidation of ethanol gas is known through two different routes depending on the acid or base properties of catalyst surface, i.e., a dehydrogenation route through CH_3CHO intermediate (on the basic surface) and a dehydration route through a C_2H_4 intermediate (on the acidic surface)[30,31].

$$C_2H_5OH \rightarrow CH_3CHO+H_2 \quad (4)$$

$$CH_3CHO(ad)+5O^-(ad) \rightarrow CO_2+2H_2O+5e^- \quad (5)$$

According to these equations, the electron donating effect of ethanol is stronger than that of the other gases. Therefore, the gas response of ethanol is higher than that of the other gases at the equivalent concentration. However, owing to the complicated reactivity of some gas molecules on the ZnO surface, the electron donating effect is not the only influential factor on gas response. Other factors (such as reaction of testing gases and sensing material, humidity, temperature, and some additional external fluctuating factor) may exist and compete against each other.

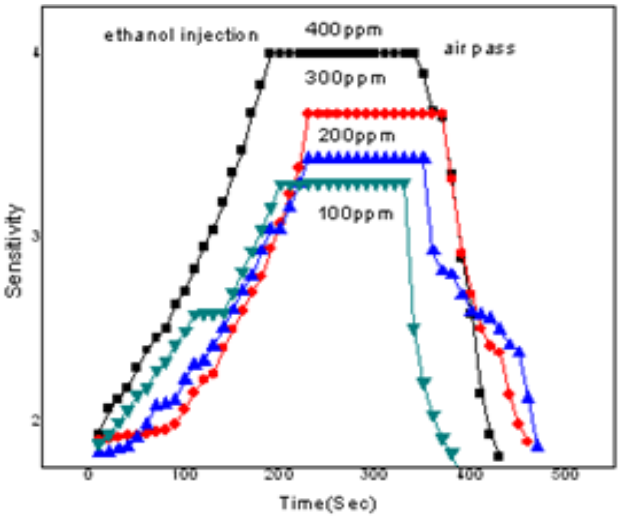

Figure 5a: Time response curve for ZnO pellet annealed at 450°C

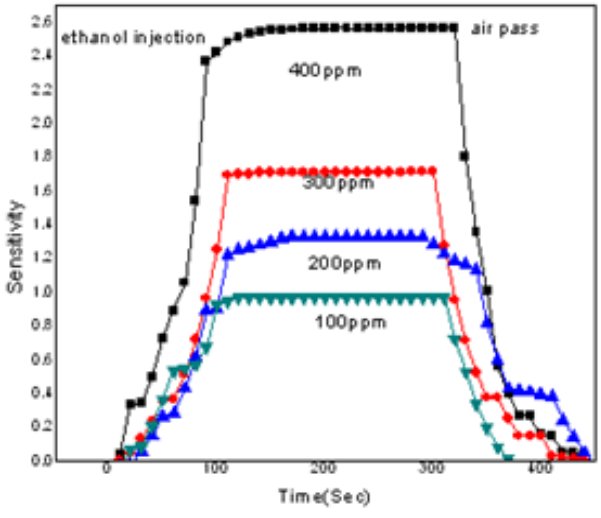

Figure 5b: Time response curve for (Mn,Co)co-doped ZnO pellet annealed at 450°C

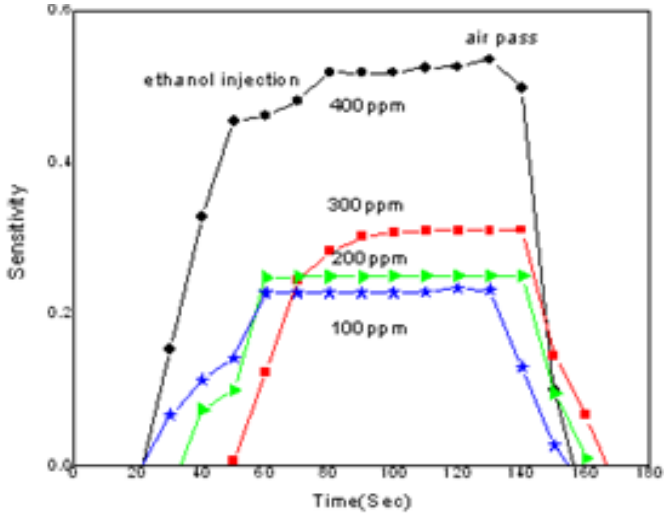

Figure 5c: Time response curve for (Mn,Co)co-doped ZnO pellet annealed at 550°C

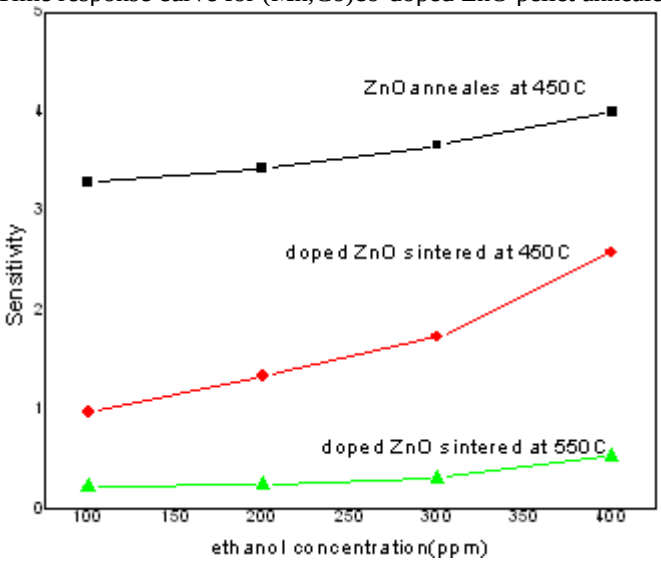

Figure 6: Ethanol concentration response curve for ZnO annealed at 450°C, (Mn,Co) codoped ZnO annealed at 450°C and 550°C

4. Conclusion:

Gas sensors were fabricated using ZnO nanoparticles subjected to a low temperature heat treatment process and their gas sensing characteristics were investigated. The morphologies of ZnO nanoparticles were observed to be rod-like particles and hexagonal structure. The crystalline sizes of ZnO hexagonal particles were found to be around 25nm. The response and recovery characteristics of the gas sensors developed herein were remarkably fast at different ethanol concentration. Their response and recovery times were 13 and 10 s, respectively. Therefore, low temperature heat treatment of nanoparticles is one of the useful methods of fabricating gas sensors having a high and fast response.

5. References:

1. T. Sahm, L. Madler, A.Gurlo, N. Barsan, S.E. Pratsinis, U. Weimar, Flame spray synthesis of tin dioxide nanoparticles for gas sensing, Sens. Actuators B 98, (2004**)** 148-153.
2. C. Xiangfeng, W. Caihong, J. Dongli, Z. Chenmou, Ethanol sensor based on indium oxide nanowires prepared by carbothermal reduction reaction, Chem. Phys. Lett. 399 (2004) 461-464.
3. O.K.Tan, W. Cao, W. Zhu, J.W. Chai, J.S.Pan, Ethanol sensors based on nano- sized α-Fe2O3 with SnO2, ZrO2, TiO2 solid solutions, Sens. Actuators B 93 (2003) 396- 401.
4. P. Ivanov, J.Hubalek, K. Prášek, X. Vilanova, E. Llobet, X. Correig, A route toward more selective and less humidity sensitive screen-printed SnO2 and WO3 gas sensitive layers, Sens. Actuators B 100 (2004) 221-227.
5. K. Galatsis, Y.X. Li, W. Wlodarski, E. Comini, G. Sberveglieri, C. Cantalini, S. Santucci, M. Passacantando, Comparison of single and binary oxide MoO3, TiO2 and WO3 sol-gel gas sensors, Sens. Actuators B 83 (2002) 276-280.

6. J. Zhang, J. Liu, Q. Peng, X. Wang, Y. Li, Nearly monodisperse Cu2O and CuO nanospheres: Preparation and applications for sensitive gas sensors, Chem. Mater. (2006) 867-871.
7. Y. Liu, J.Dong, P.J. Hesketh, M. Liu,. Synthesis and gas sensing properties of ZnO single crystal flakes, J. Mater. Chem. 15 (2005) 2316-2320.
8. C.Liewhiran, S. Phanichphant, Influence of thickness on ethanol sensing characteristics of doctor-bladed thick film from flame-made ZnO nanoparticles, Sensors 7 (2007**)** 185-201.
9. H. Xu, X. Liu, D. Cui, M. Li, M.A. Jiang, novel method for improving the performance of ZnO gas sensors, Sens. Actuators B 114 (2006**)** 301-307.
10. P.P.Sahay, S. Tewari, S. Jha, M. Shamsuddin, Sprayed ZnO thin films for ethanol Sensor, J. Mater. Sci. 40 (2005) 4791-4793.
11. C. Xiangfeng, J. Dongli, A.B. Djurišic, Y.H. Leung, Gas-sensing properties of thick film based on ZnO nano-tetrapods, Chem. Phys. Lett. 401 (2005) 426-429.
12. N.J.Dayan, R.N. Karekar, R.C. Aiyer, S.R. Sainkar, Effect of film thickness and curing temperature on the sensitivity of ZnO:Sb thick-film hydrogen sensor, J. Mater. Sci. - Mater. Electron. 8 (1997**)** 277-279.
13. L. Zheng, T. Xu, G. Li, Q. Yin, Influence of thickness on oxygen-sensing properties of TiO2 thin films on Al2O3, Jpn. J. Appl. Phys., Part 141 (2002)4655- 4658.
14. Y.L.Lee, C.Y. Sheu, R.H. Hsiao, Gas sensing characteristics of copper phthalocyanine films; effects of film thickness and sensing temperature, Sens. Actuators B 99 (2004) 281-287.
15. F. Hossein-Babari, M. Orvatinia, Analysis of thickness dependence of the sensitivity in thin film resistive gas sensors, Sens. Actuators B 89 (2003) 256-261.
16. So-Jung kim, Dong-wha park, Preparation of ZnO nanopowders by thermal plasma and characterization of photo-catalytic property, Appl. Surf. Sci. 255 (2009) 5363- 5367.
17. Babita Baruwati, D.Kishore kumar, Sunkara V. Manorama, Hydro thermal synthesis of highly crystalline ZnO nanoparticles: A competitive sensor for LPG and EtOH, Sens.Actuators B 119 (2006) 676-682.
18. B.C.Yadav, Richa srivastava, C.D. Dwivedi, P.Pramanik, Synthesis of nanosized ZnO using dropwise method and its performance as moisture sensor, Sensors and actuators A 153 (2009) 137-141.
19. O.Lopatiuk, L. Chernyak, Lithium related states as deep electron traps in ZnO, Appl.Phys.Lett. 87 (2005) 2144110-2144112.
20. Y. Ohbuchi, T.Kawahara, Y.Okamoto, J.Morimoto, Characterization of interface states in degraded ZnO varistors, Jpn. J. Appl. Phys. 41 (2002) 190.
21. S. Wabanz, A.A.Kornyshev, Proton transport in polarized water, J. Chem. Phy. 114 (2001) 10039-10048.
22. P.K. Jain, N.S.Saxeena, Temperature and composition dependence of electrical conductivity of Se90In10-xSbx (x=0, 2, 4, 6, 8, 10) chalcogenide glasses, Journal of Non – Oxide and Photonic Glasses, 1(2009) 43-52.
23. B.C.Yadav, Richa srivastava, C.D.Dwivedi, P.Pramanik, moisture sensor based on ZnO nanomaterial synthesized through oxalate route, Sensors and actuators B 131 (2008) 216-222.
24. R.Ananda Kumari, R.Chandramani**,** Electrical conductivity and dielectric measurements in Au^{+} doped/undoped KDP crystals with KCl and NaCl as additives, Indian journal of pure and applied physics, 43 (2005) 123-128.
25. M. Serina, D. Sakar, O. Cankurtaran, F. Karaman, Analysis of polyarylate Ardel D -100 films undoped and doped By BF^{-}_{4} as a function of the doping concentration, Journal of Optoelectronics and Advanced Materials 7 (2005) 1533 – 1538.
26. Jin Hyung Juna, Junggwon Yuna, Kyoungah Choa, In-Sung Hwangb, Jong-Heun Leeb, Sangsig Kima Necked ZnO nanoparticle-based NO2 sensors with high and fast response, Sensors and Actuators B 140 (2009) 412–417
27. X.L.Cheng, H. Zhao, L.H. Huo, S. Gao, J.G. Zhao, ZnO nanoparticulate thin film: preparation, characterization and gas-sensing property, Sens. Actuators B 102 (2004) 248-252.
28. J.Q. Xu, J.J. Han, Y. Zhang, Y.A. Sun, B. Xie, Sens. Studies on alcohol sensing mechanism of ZnO based gas sensors, Sens. and Actuators B 132 (2008) 334-339.
29. S.R. Morrison, Selectivity in semiconductor gas sensors, Sens. Actuators B 12 (1987) 425-440.
30. N. Yamazoe, G. Sakai, K.Shimanoe, Oxide semiconductor gas sensors, Catal. SurV. Asia 7 (2003**)** 63-75.
31. T. Jinkawa, G. Sakai, J. Tamaki, N. Miura, N. Yamazoe, Relationship between alcohol gas sensitivity and surface catalytic property of tin oxide sensors modified with acidic or basic oxides, J. Mol. Catal. A 155 (2000) 193–200.